

pubs.acs.org/acsapm Forum Article

Fouling- and Chlorine-Resistant Nanofiltration Membranes Fabricated from Charged Zwitterionic Amphiphilic Copolymers

Samuel J. Lounder and Ayse Asatekin*



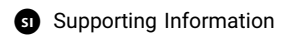
Cite This: https://doi.org/10.1021/acsapm.1c01940



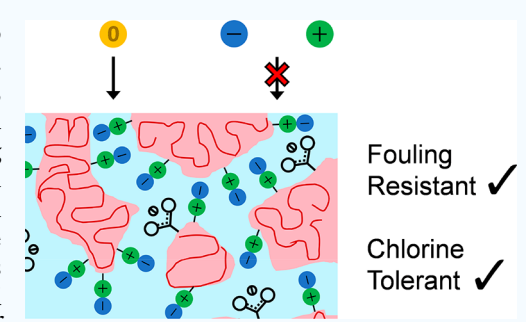
ACCESS

Metrics & More





ABSTRACT: New polymer chemistries are urgently needed to develop nanofiltration (NF) membranes with improved fouling and chlorine resistance. This work introduces charged zwitterionic amphiphilic copolymers (CZACs), self-assembling terpolymers that spontaneously form a network of ~1–2 nm hydrophilic nanochannels composed of zwitterionic and acidic/ ionizable building blocks. We leverage CZAC self-assembly to develop membrane filters with anionic nanopores, thereby enabling enhanced salt rejection through Donnan exclusion (R(Na₂SO₄) = 93.6% at 5 mM). The CZAC membranes demonstrate hydraulic permeability comparable to commercial nanofiltration membranes (0.86 – 2.3 L μ m m⁻² h⁻¹ bar⁻¹), exceptional fouling resistance, and a high level of chlorine tolerance (32 000 ppm·h), addressing key performance limitations of current NF membranes.



KEYWORDS: membrane, self-assembly, ion separation, fouling resistance, chlorine tolerance

1. INTRODUCTION

The development of advanced water treatment technologies is crucial for addressing environmental stresses and water scarcity. $^{1-3}$ Membranes represent a low footprint and effective option for water treatment, finding utility within the municipal, industrial, and commercial areas. $^{1,2,4-7}$ Reverse osmosis (RO) membranes, for instance, enable the production of safe drinking water for communities with limited access to potable water sources. 2,4,6,8 Nanofiltration (NF) membranes, defined by an effective pore size of ~ 1 nm, can be used to remove divalent salts from water and wastewater streams in applications such as water softening 9,10 and sulfate removal for oil recovery. 9,11

Most commercial RO and NF membranes are thin film composites (TFCs) featuring cross-linked polyamide selective layers (PA-TFCs). 12 Having been in commercial use for decades, PA-TFCs are well-optimized and offer reasonably high water permeability along with the desired divalent salt rejection.¹³ However, polyamide selective layers also come with significant limitations inherent to their chemical structure. For instance, polyamide offers low resistance to fouling, ¹⁴ defined by undesired adsorption and accumulation of feed components on the membrane surface or in the membrane pores. Membrane fouling can have a detrimental effect on membrane performance, substantially limiting water permeance/ membrane lifetime and necessitating chemical treatment for its reversal. 14-21 Additionally, polyamide is sensitive to chlorine degradation. 4,13,22-24 This prevents the use of hypochlorite for biofouling management, necessitating complex staged treatment and/or alternative oxidizing agents. 4,13,22

While several groups have attempted to mitigate these issues through surface functionalization and/or by modifying the monomers used to form the polyamide selective layer, ^{1,25–27} the development of new polymer chemistries with inherent fouling and chlorine resistance would offer a simple and more sustainable solution. Membranes derived from polyelectrolyte multilayers (PEMs) represent one example of this (*e.g.*, Pentair X-Flow HFW 1000^{28,29}), although PEM membranes typically suffer the drawbacks of complex manufacturing³⁰ and low stability in high ionic strength solutions.³¹

Random zwitterionic amphiphilic copolymers (r-ZACs) are random/statistical copolymers of hydrophobic and zwitterionic building blocks. Due to favorable interactions between neighboring zwitterions, r-ZACs can self-assemble to form a bicontinuous network featuring zwitterionic nanochannels surrounded by a hydrophobic nanodomain.^{32–35} The zwitterionic nanochannels permeate water and small solutes, while the hydrophobic nanodomain acts as the pore wall.

Our group prepared the first generation of r-ZAC membrane filters by coating an $\sim 1~\mu$ m-thick copolymer layer onto a porous support. The effective pore size of these membranes was $\sim 1-2$ nm, corresponding to an ~ 1000 g/mol molecular weight cutoff and relatively low salt

Special Issue: Polymer Membranes for Precision

Separations

Received: December 31, 2021 Accepted: February 22, 2022



retention. 36,37 Due to the hydrophilicity of the zwitterionic nanochannels, the r-ZAC membranes exhibited exceptional fouling resistance, suffering no irreversible loss in flux when challenged with model proteins, organic biomacromolecules, and oil emulsions. 15,36,37 These r-ZAC membranes were also stable upon chlorine treatment, 15 allowing the use of hypochlorite for facile management of biofouling. However, these r-ZAC membranes also exhibited relatively low salt rejection due to the $\sim 1-2$ nm pore size combined with the overall neutral chemistry of the membrane selective layer. 15,36 More recently, we have developed a cross-linking approach to limit the aqueous swelling of the zwitterionic nanochannels. 38,39 This allowed for controllable reductions in membrane pore size, down to an effective pore size of < 1.0 nm, while retaining the excellent fouling resistance of previous r-ZACs. However, the most highly cross-linked samples exhibit significant ion selectivity, cross-linking also reduces the permeance to quite low values. Therefore, there is a need for novel r-ZACs that combine the fouling and chlorine resistance offered by this chemical approach with rejection profiles that mirror commercial NF membranes in applications such as water softening⁹ and sulfate removal for oil recovery^{9,11} while retaining commercially relevant permeances. Furthermore, expansion of available r-ZAC chemistries can potentially enable new self-assembled pore functionalities for developing membrane filters with advanced and targeted selectivity.

In this work, we develop membranes that combine NF-type selectivity with fouling and chlorine resistance by modifying the r-ZAC polymer family to improve salt rejection. For this purpose, we synthesized the first charged zwitterionic amphiphilic copolymers (CZACs), random/statistical terpolymers combining hydrophobic, zwitterionic, and acidic, ionizable building blocks. Similar to r-ZACs, we show that CZACs self-assemble to form a bicontinuous network featuring 1-2 nm hydrophilic nanochannels comprised mostly of the zwitterionic and ionizable repeat units, surrounded by hydrophobic nanodomains. We demonstrate that CZACs and r-ZACs function analogously as membrane selective layers, permeating water and other solutes through the hydrophilic nanochannels. We show that while CZAC and r-ZAC membranes possess equal nanochannel diameter, CZAC nanochannels are negatively charged due to the deprotonation of the acidic repeat unit. This enhances the rejection of salts through Donnan exclusion. We model the rejection properties of these membranes using the Donnan Steric Pore Model (DSPM), 40,41 and we discuss mechanisms of rejection as well as potential applications. Due to the presence of zwitterionic groups, CZAC membranes are highly resistant to fouling by proteins and organic macromolecules. This polymer chemistry also enables high chlorine resistance, with negligible changes in performance upon exposure to chlorine (32 000 ppm·h). While this first report demonstrates the use of CZACs as NF membrane selective layers, we expect further modification and optimization of polymer chemistry and coating processes will lead to further enhanced performance and better control over selectivity to enable their use in additional applications.

2. EXPERIMENTAL SECTION

2.1. Copolymer Synthesis. All copolymers were synthesized by free radical polymerization (FRP). Copolymer composition was determined ¹H NMR spectroscopy (DMSO-*d*₆, 500 MHz, Figure S1). *2.1.1. Synthesis of P(TFEMA-r-SBMA) 60:40 (ZAC-0).* First, sulfobetaine methacrylate (SBMA, 12.0 g), LiCl (0.3 g), and dimethyl

sulfoxide (DMSO, 240 mL) were added to a 500 mL round-bottom (RB) flask. The temperature was then raised to 70 °C for 1 h to aid in dissolving the zwitterionic monomer and afterward returned to room temperature. We then added trifluoroethyl methacrylate (TFEMA, 18.0 g) and azobisisobutyronitrile (AIBN, 30 mg) to the RB flask. Next, the flask was sealed with a rubber septum, purged with nitrogen for 20 min, and placed in a 70 °C oil bath with stirring. After 20 h, the reaction was terminated by exposure to air and addition of 4-methoxy phenol (MEHQ, 1.5 g). To precipitate the copolymer, we poured the solution into 2400 mL of 1:1 ethanol:hexane. The copolymer was then cut into small pieces and washed three times in 1:1 ethanol:hexane. After several days of air drying, the copolymer was dried under vacuum at 50 °C for 24 h. The yield was approximately 60%.

2.1.2. Synthesis of P(TFEMA-r-SBMA-r-MAA) 60–28–12 (CZAC-1). First, SBMA (2.61 g), LiCl (0.090 g), and DMSO (80 mL) were added to a 250 mL RB flask. The temperature was then raised to 70 °C to aid in dissolving the zwitterionic monomer and afterward returned to room temperature. We then added TFEMA (5.49 g), methacrylic acid (MAA, 1.11 g), and AIBN (11 mg) to the RB flask. Next, the flask was sealed with a rubber septum, purged with nitrogen for 20 min, and placed in a 70 °C oil bath with stirring. After 20 h, the reaction was terminated by exposure to air and addition of MEHQ (0.5 g). To precipitate the terpolymer, we poured the solution into 800 mL of 1:1 ethanol:hexane. The terpolymer was then cut into small pieces and washed two times in 1:1 ethanol:hexane. After several days of air drying, the terpolymer was dried under vacuum at 50 °C for over 24 h. The yield was 38%.

2.1.3. Synthesis of P(TFEMA-r-SBMA-r-MAA) 53–28–19 (CZAC-2). First, SBMA (2.80 g), LiCl (0.10 g), and DMSO (90 mL) were added to a 250 mL RB flask. The temperature was then raised to 70 °C to aid in dissolving the zwitterionic monomer and afterward returned to room temperature. We then added TFEMA (5.30 g), MAA (1.90 g), and AIBN (9.8 mg) to the RB flask. Next, the flask was sealed with a rubber septum, purged with nitrogen for 20 min, and placed in a 70 °C oil bath with stirring. After 20 h, the reaction was terminated by exposure to air and the addition of MEHQ (0.7 g). To precipitate the terpolymer, we poured the solution into 900 mL of 1:1 ethanol:hexane. The terpolymer was then cut into small pieces and washed three times in 1:1 ethanol:hexane. After several days of air drying, the terpolymer was dried under vacuum at 50 °C for over 24 h. The yield was 60%.

2.2. Differential Scanning Calorimetry (DSC). To characterize terpolymer self-assembly, we performed temperature modulated DSC (TMDSC) using a TA Q100 series calorimeter (TA Instruments) equipped with a refrigerated cooling system and purged with nitrogen at 50 mL/ min. We sealed 3–6 mg of terpolymer in an aluminum DSC pan for each experiment. In the instrument, we equilibrated each sample at 120 °C for 15 min to condition the samples. For each modulated thermal cycle, temperature was increased by heating from -80 to +230 °C at 3 °C/ min while modulating \pm 1.5 °C/ min. We cooled to -80 °C at the end of the first modulated ramp and to 25 °C at the end of the second modulated ramp. The glass transition temperature (T_g) was taken as the midpoint of the baseline shift from the second run.

We used the Fox equation to calculate the T_g predicted for the terpolymer as a homogeneously mixed single phase: 37

$$T_{g,Fox} = \left(\frac{w_{PTFEMA}}{T_{g,PTFEMA}} + \frac{w_{PSBMA}}{T_{g,PSBMA}} + \frac{w_{PMAA}}{T_{g,PMAA}}\right)^{-1}$$
(1)

Here w_i and $T_{g,i}$ are the weight fraction and homopolymer T_g of component i, respectively. The homopolymer T_g s were $T_{g,PTFEMA} = 84$ °C, $T_{g,PSBMA} = 220$ °C, $T_{g,PSBMA} = 220$ °C, and $T_{g,PMAA} = 230$ °C.

2.3. Membrane Fabrication. Copolymers were first dissolved in trifluoroethanol to prepare 10 w/v% solutions. The solutions were then passed through a 1.2 μ m syringe filter, degassed at 50 °C, and cooled to room temperature. We then coated the copolymer solutions onto a commercial PES ultrafiltration membrane (UE50, Trisep) using a wire wound rod (#6, Gardco). The coated membranes were

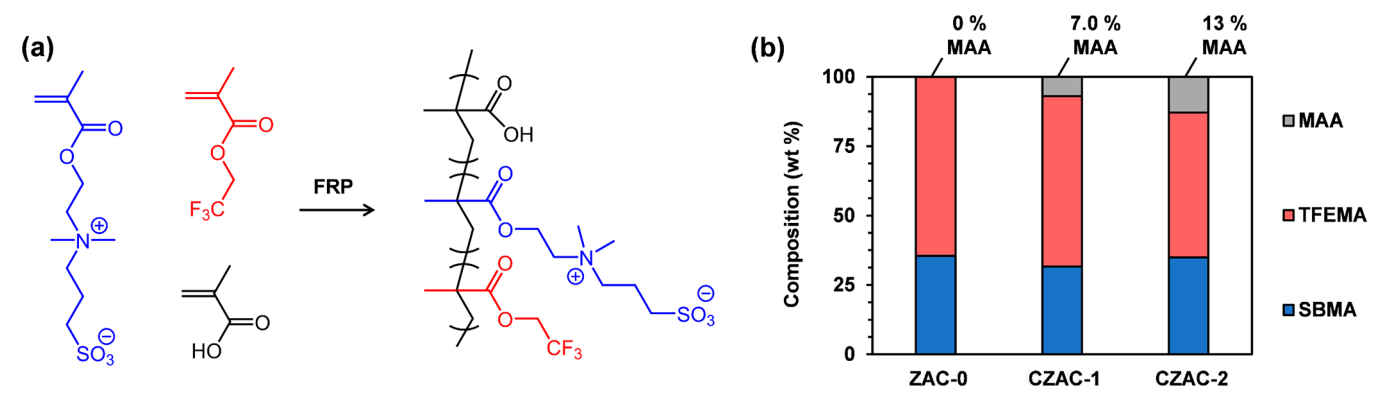


Figure 1. (a) Synthesis scheme for the CZAC used in this study, P(TFEMA-r-SBMA-r-MAA), via free radical polymerization (FRP). (b) Composition of the studied copolymers. CZAC-1 and CZAC-2 were CZACs of varying MAA content, while ZAC-0 was a neutral r-ZAC used as a control.

left undisturbed for ~ 10 s and then plunged into a nonsolvent bath of IPA for 20 min. Membranes were then transferred to distilled water for at least 12 h prior to further testing.

2.4. Characterization of Membrane Morphology. We performed scanning electron microscopy (SEM) to characterize the membrane layer morphology. To prepare the samples, membrane sections were freeze-fractured and sputter-coated with gold—palladium. SEM images of the membrane cross-section were obtained using a Phenom G2 pure tabletop SEM at a 5 kV setting with 19 000× magnification.

2.5. Filtration Tests and Donnan Steric Pore Model (DSPM). Filtration experiments were performed using 10 mL Amicon 8010 stirred cells in dead-end mode. The membrane disk area was 4.1 cm². The pressure was 50 psi unless otherwise specified. The feed solutions had a consistent pH of 5.5, except for those where we reduced the pH by pipetting small volumes of $H_2SO_{4(aq)}$. To measure membrane permeance, we tracked permeate flux (J_w) at a known pressure (ΔP) using Ohaus Scout Pro scales linked with a computer. Permeance (L_P) was determined by:

$$L_{p} = \frac{J_{w}}{\Delta P} \tag{2}$$

When appropriate, we accounted for osmotic pressure (eq S2). Hydraulic permeability (P_{wH}) of each membrane selective layer, defined as water flux (J_w) normalized by the driving force for water permeation ($\Delta P/\delta$), was calculated using

$$P_{wH} = \frac{J_w \delta}{\Delta P} = L_p \delta \tag{3}$$

where δ is the thickness of the membrane selective layer. To measure rejection, we loaded 10.0 mL of solution into the filtration cells, filtered 1.5 mL, and then collected an additional 0.7 mL of permeate for analysis. Rejection (R) was determined by

$$R = \left(1 - \frac{C_p}{C_F}\right)100\% \tag{4}$$

where C_P and C_F are the feed and permeate concentrations, respectively. Equation 4 does not account for concentration polarization, which was shown to be negligible (Supporting Information). The rejection of neutral solutes and salts was modeled using the DSPM. 40,41 We followed the approach laid out by Bowen, 40,41 although we calculated the hindered diffusive and convective transport using Deen's hydrodynamic theory 43 (Supporting Information). This continuum model treats the membrane as an array of cylinders of diameter D_p and anionic charge density χ . Each solute is treated as a sphere with a diameter equal to its Stokes radius.

To model membrane performance using the DSPM, we used Mathcad Prime to numerically solve rejection as a function of D_p , χ , and solute parameters (Supporting Information). To determine D_p ,

we filtered solutions of glucose (300 ppm), maltose (300 ppm), α-cyclodextrin (300 ppm), β-cyclodextrin (300 ppm), and vitamin B12 (100 ppm) and used an R^2 minimization algorithm to fit the pore diameter that best predicted rejection (Supporting Information). To model salt rejection, we filtered Na₂SO₄, Li₂SO₄, CaSO₄, MgSO₄, NaCl, and LiCl at feed concentrations of 1 mM and 5 mM and used a similar R^2 minimization algorithm to fit the anionic charge density that best predicted salt rejection at a given feed concentration (Supporting Information).

2.6. Fouling Studies. Fouling tests were performed using the same dead-end filtration setup described above. To determine protein fouling resistance, we used 1000 ppm solutions of bovine serum albumin (BSA) with 10 mM CaCl₂ (pH 6.3). A 10 mM CaCl₂ solution was selected as the background solution to enhance fouling propensity. To determine organic fouling resistance, we used solutions of humic acid and sodium alginate (1000 ppm each). We reduced the pH to 4.5 using $HCl_{(aq)}$ to enhance fouling propensity. To determine organic fouling propensity.

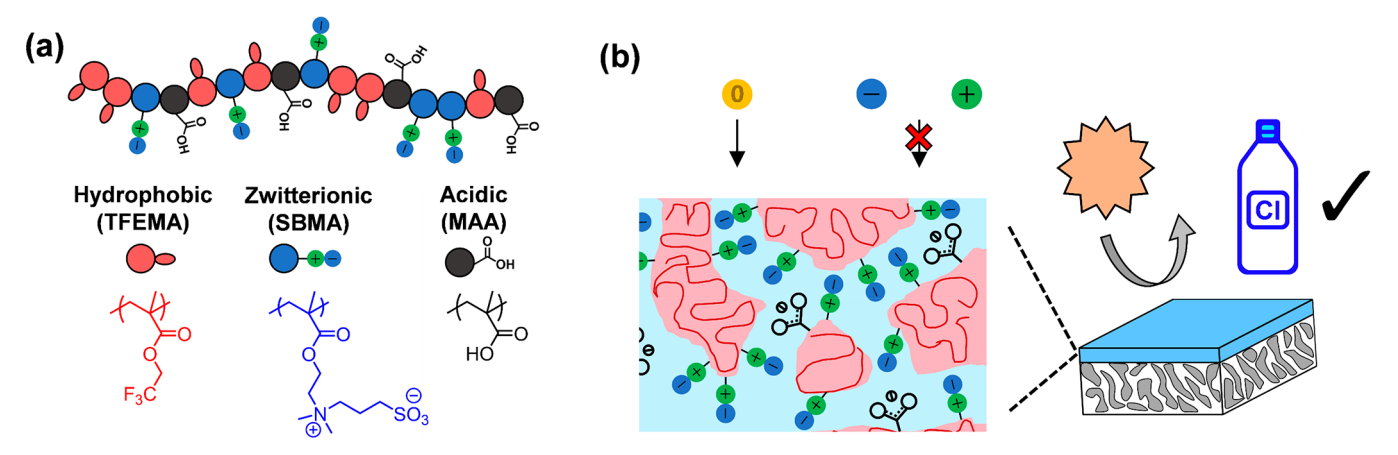
The CZAC TFC membrane fouling experiments were performed at 50 psi operating pressure. For a given test, we first determined the initial flux (J_0) of the CZAC membranes using the corresponding background solution of the fouling mixture. We measured $J_0 = 5.4 \text{ L}$ m^{-2} h^{-1} and $J_0 = 8.1$ L m^{-2} h^{-1} for the protein and organic fouling experiments, respectively. We then charged the filtration cell with the fouling solution and filtered the foulant for either 24 or 20 h. During the fouling period, we tracked flux (I) vs time. As permeate passed through the membrane, the depleted volume of fouling solution was replenished with fresh fouling solution by attaching the cell to a pressurized dispensing vessel containing the foulant. At the end of the fouling period, we emptied the cells and gently rinsed with the background solution before measuring the final flux. We repeated identical fouling experiments using commercial NF membranes as controls, except that we adjusted the pressure to result in the same initial flux that was measured for the CZAC membranes.

2.7. Chlorine Tolerance. For accelerated chlorine exposure, we immersed membrane disks in a 2,000 ppm solution of sodium hypochlorite for 16 h (32 000 ppm·h chlorine exposure). The pH was adjusted to 4.5 using HCl to ensure that hypochlorous acid was the active chlorine species. To verify that chlorine levels remained constant, we measured the concentration of $500 \times$ dilutions of the chlorine solution before and after the treatment using chlorine test strips (0-10 mg/L range, Aquachek).

To determine the effect of chlorine exposure on membrane performance, we compared rejection of 5 mM $\mathrm{Na_2SO_4}$ ($R(\mathrm{Na_2SO_4})$) and permeance (L_P) before and after chlorine treatment. Membrane permeance after chlorine treatment ($L_{P,After}$) was normalized by the initial permeance before chlorine treatment ($L_{P,Before}$).

To determine the effect of chlorine exposure on terpolymer bond chemistry, we performed attenuated total reflectance Fourier transform infared (ATR-FTIR) spectroscopy using an FT/IR-6200 spectrophotometer (JASCO Corp) equipped with a ZnSe crystal (4000–600 cm⁻¹, 4 cm⁻¹ resolution, 32 scans). We compared the

Scheme 1. (a) Polymer Architecture/Chemistry of the Charged Zwitterionic Amphiphilic Copolymer (CZAC) Used in This Study, P(TFEMA-r-SBMA-r-MAA), and (b) Schematic Showing the CZAC Nanostructure^a



"The terpolymer self-assembles to form hydrophilic nanochannels (blue) surrounded by the hydrophobic nanodomain (red). Zwitterions and deprotonated acidic groups partition into the hydrophilic nanochannels. The negative charge of the carboxylate groups enhances salt rejection by the Donnan exclusion mechanism, and the hydrophilicity of the zwitterions grants excellent fouling resistance. Due to stable bond chemistry, the CZAC TFC membranes are also tolerant to chlorine exposure.

Table 1. Reaction Mixture Compositions, Copolymer Physical Properties, and Properties of the Prepared Membranes

ZAC-0	CZAC-1	CZAC-2
TFEMA: 60	TFEMA: 60	TFEMA: 53
SBMA:40	SBMA: 28	SBMA: 28
	MAA: 12	MAA: 19
TFEMA: 64	TFEMA: 61	TFEMA: 52
SBMA: 36	SBMA: 32	SBMA: 35
MAA	MAA: 7.0	MAA: 13
60	38	60
173 ^a	165	175
129 ^b	127 ^b	139 ^b
1.41 ± 0.23^{c}	1.66 ± 0.18^{c}	2.23 ± 0.44^{c}
0.61 ± 0.07^{c}	0.62 ± 0.03^{c}	1.03 ± 0.14^{c}
0.86 ± 0.17^d	1.02 ± 0.12^d	2.29 ± 0.55^d
	SBMA:40 TFEMA: 64 SBMA: 36 MAA 60 173^a 129^b 1.41 ± 0.23^c 0.61 ± 0.07^c	TFEMA: 60 SBMA: 40 SBMA: 28 MAA: 12 TFEMA: 64 SBMA: 36 SBMA: 32 MAA MAA: 7.0 60 38 173^a 165 129^b 1.41 ± 0.23^c 0.61 ± 0.07^c 0.62 ± 0.03^c

"Reported by ref 37. "Calculated using eq 1. "Uncertainty (ε_{Lp} or ε_{δ}) reported as the 95% confidence interval calculated using multiple measurements. "Uncertainty (ε_{PwH}) calculated using propagations of error analysis: 49 ε_{PwH} = $[(L_P * \varepsilon_{\delta})^2 + (\delta * \varepsilon_{Lp})^2)]^{0.5}$.

ATR-FTIR spectra of as cast and chlorine-treated terpolymer films. We defined the average intensity ranging from $1950-1850~\rm cm^{-1}$ as the baseline and normalized the spectra using the height of the carbonyl peak $(1740-1737~\rm cm^{-1}).^{37,46}$ The terpolymer films were prepared by aerially drying a 10 w/v% solution of terpolymer/trifluoroethanol in a Teflon dish.

3. RESULTS AND DISCUSSION

3.1. Copolymer Synthesis. To develop r-ZACs with anionic functionality, i.e. CZACs, we synthesized random terpolymers of TFEMA, SBMA, and MAA by FRP (Figure 1a). The hydrophobic (TFEMA) and zwitterionic (SBMA) building blocks served to form hydrophilic nanochannels through r-ZAC self-assembly, while the acidic repeat unit (MAA) served to provide negative charge to the nanochannels upon deprotonation in aqueous solution (Scheme 1b). To study the effect of acidic repeat unit content on self-assembly and membrane performance, we synthesized three copolymers of varying compositions: ZAC-0, CZAC-1, and CZAC-2 (Figure 1b, Table 1). The content of the acidic repeat unit (MAA) ranged 0-13 wt %, while the content of the zwitterion (SBMA) remained mostly constant (32-36 wt %). The hydrophobic repeat unit (TFEMA) composed the

remaining weight fraction (64 - 52 wt %). CZAC-2 had almost twice the MAA content as CZAC-1.

For all three copolymers, the final copolymer composition was similar to the initial composition of the reaction mixture (Table 1). This suggests a near-random repeat unit sequence, consistent with the polymer architecture of previously investigated self-assembling r-ZACs. This result was unsurprising for the CZAC-1 and CZAC-2 terpolymers, because previous work shows that copolymers of TFEMA with SBMA³⁷ and TFEMA with MAA⁴⁷ also possess a near-random repeat unit sequence. It is worth mentioning that there are strict kinetic requirements for a terpolymer to be truly random, so it is likely that the terpolymers were somewhat graded and/or blocky. Despite this caveat, we will refer to these terpolymers as random to stay consistent with the terminology appearing in the published literature.

3.2. Characterization of CZAC Self-Assembly. To study terpolymer nanostructure, we performed TMDSC (Figure 2, Table 1). Both CZACs exhibited a single T_g (CZAC-1, T_g = 165 °C; CZAC-2, T_g = 175 °C) that did not correspond to a homopolymer phase ($T_{g,PTFEMA}$ = 84 °C, 37 $T_{g,PSBMA}$ = 220 °C, 37 and $T_{g,PMAA}$ = 230 °C, 42). Additionally, the single T_g s were significantly greater than Fox equation prediction for if the

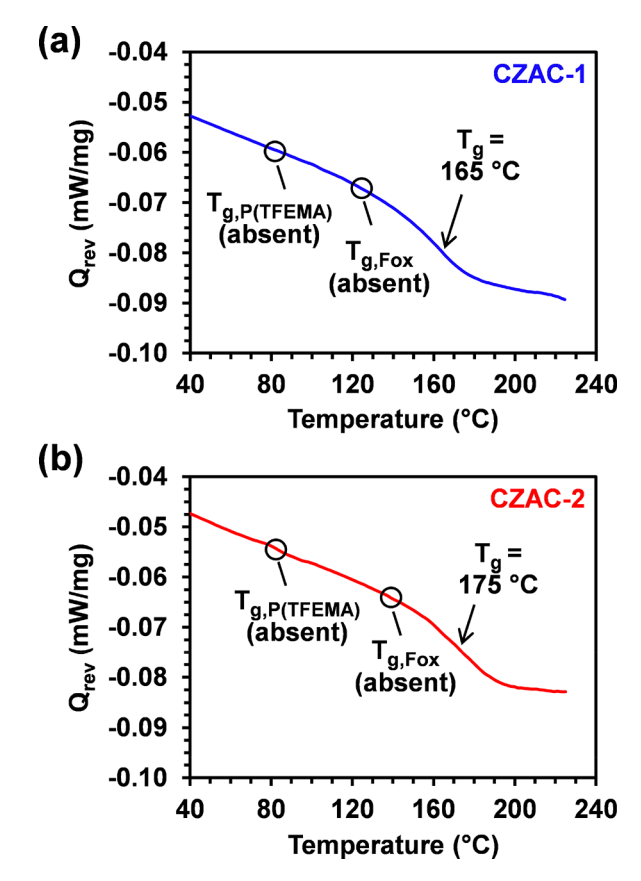


Figure 2. (a) TMDSC thermograms for (a) CZAC-1 and (b) CZAC-2 (second run, 3 °C/min heating ramp, \pm 1.5 °C/min modulation). For both CZACs, we observed a single T_g corresponding to the glass transition of the hydrophilic nanodomain.

terpolymers were homogenously mixed as a single phase (eq 1, Table 1). These results imply that the single T_g s correspond to a glassy nanodomain enriched in SBMA and MAA.^{34,37} This

domain likely limits the mobility of chain segments in the bordering TFEMA-rich hydrophobic domain due to a high degree of interconnectivity, thereby obscuring a lower temperature glass transition. These results are consistent with the behavior of self-assembling r-ZACs without weakly acidic groups, where the single $T_{\rm g}$ s correspond to a zwitterion-rich nanodomain.

3.3. Fabrication of Thin Film Composite (TFC) Membranes. Thin film composite (TFC) membranes were prepared by coating a solution of each copolymer in trifluoroethanol onto a porous PES ultrafiltration membrane support (UE50, Trisep) followed by immersion into a nonsolvent coagulation bath. This well-established membrane fabrication technique is readily scalable to roll-to-roll manufacturing. The resulting selective layer thicknesses ranged between 0.61 and 1.0 μ m, as determined by SEM cross-sectional images (Figure 3, Table 1). The ZAC-0 and CZAC-1 membranes had similar selective layer thicknesses (0.61–0.62 μ m), while the selective layers of the CZAC-2 membranes were somewhat thicker (1.0 μ m). We expect that this difference was due to slight variations in the evaporation time and/or differences in polymer–nonsolvent affinities. S1

3.4. Permeance and Hydraulic Permeability. For the ZAC-0, CZAC-1, and CZAC-2 membranes, membrane permeances and selective layer hydraulic permeabilities ranged between 1.4–2.2 and 0.86–2.3 L μm m⁻² h⁻¹ bar⁻¹, respectively (Table 1). Higher permeance and hydraulic permeability corresponded to TFC membranes with greater MAA content. The total weight fraction of hydrophilic components (SBMA and MAA) also increased with increasing MAA content, so it is possible that the higher permeance and hydraulic permeability was due to a greater volume fraction of hydrophilic nanochannels. We urge caution in analyzing this trend, however, because numerous factors (*e.g.*, humidity, evaporation time, and polymer–nonsolvent affinities) likely affect the permeances and selective layer hydraulic permeabilities of these TFC membranes.

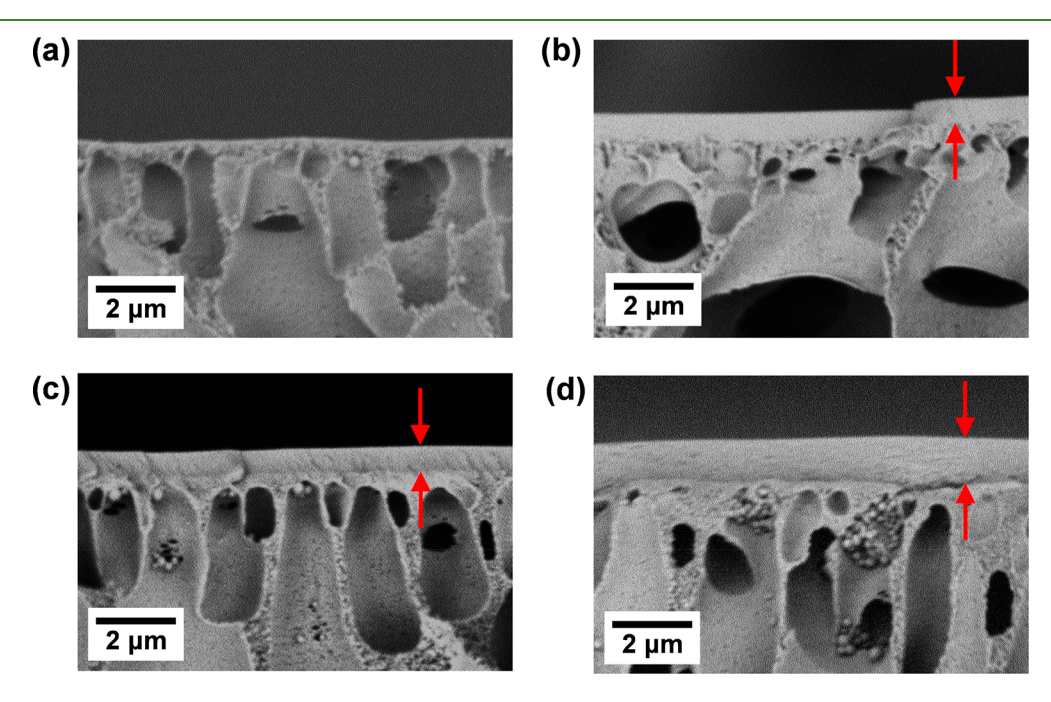


Figure 3. SEM cross-sectional images of (a) the uncoated support membrane (Trisep UE50) and (b-d) coated TFC membranes featuring dense copolymer selective layers: (b) ZAC-0, (c) CZAC-1, and (d) CZAC-2.

The CZAC membranes had lower permeances than most PA-TFC NF membranes. 52 Permeance is inversely proportional to membrane selective layer thickness, however, and the CZAC membranes had much thicker selective layers (0.6-1.0 μ m) than PA-TFCs (~0.1 μ m)³⁷ due to the different membrane fabrication methods. Hydraulic permeability quantifies water flux normalized by the pressure driving force for permeation (eq 3), and therefore provides a better metric for comparing the inherent rate of water transport through a membrane material. 53,54 CZAC membrane selective layer hydraulic permeability (0.86 – 2.3 L μ m m⁻² h⁻¹ bar⁻¹) was slightly greater than that of typical PA-TFC NF membrane selective layers $(0.3 - 1.8 \text{ L} \mu \text{m} \text{ m}^{-2} \text{ h}^{-1} \text{ bar}^{-1}).^{37}$ This indicates that CZAC TFC membranes manufactured with thinner selective layers could have comparable or higher permeances than state-of-the-art PA-TFC membranes. Previous work has demonstrated the fabrication of r-ZAC TFC membranes with exceptionally thin (\sim 0.1–0.2 μ m) selective layers and ultrahigh permeance, 55,56 suggesting that higher permeance could also be realized for CZAC TFC membranes.

3.5. Effect of Copolymer Composition on Size-Based Selectivity. To compare the size-based selectivity of the ZAC-0, CZAC-1, and CZAC-2 membranes, we filtered aqueous solutions of three neutral solutes of varying sizes (Figure 4a). Concentration polarization was neglected, as it was shown to

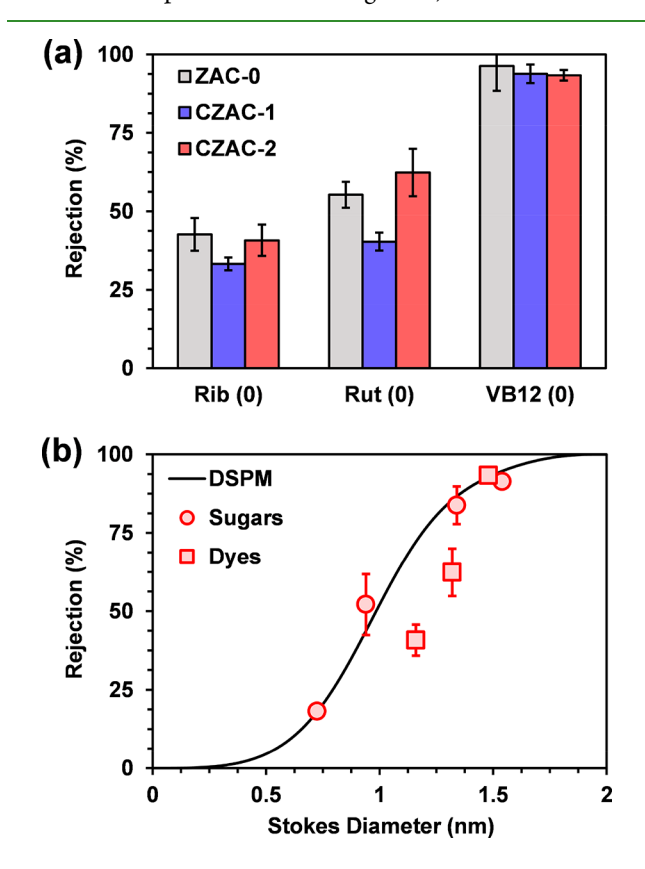


Figure 4. (a) Rejection of neutral solutes by the ZAC-0, CZAC-1, and CZAC-2 membranes (Rib, riboflavin; Rut, rutin hydrate; VB12, vitamin B12). (b) CZAC-2 membrane rejection of various neutral solutes versus Stokes diameter (sugars glucose, maltose, α -cyclodextrin, and β -cyclodextrin; dyes riboflavin, rutin, and vitamin B12). The solid line is the DSPM fit to the rejection of sugars and vitamin B12 ($D_p = 1.95$ nm, Table S1). The error bars appearing in parts a and b are the 95% confidence interval calculated using Student's t-distribution.

be negligible (Figure S2). We observed similar neutral solute rejections for the three membranes, suggesting that MAA had no measurable influence on the effective membrane pore size. We further investigated the size-based selectivity of the CZAC-2 membrane, which had the highest MAA content, by filtering neutral solutes of known Stokes diameter (Figure 4b, Table S1). The Stokes diameter accounts for the size of the solute plus its hydration shell, making it a good general measure of size. 40,41,57 The CZAC-2 membranes retained β -cyclodextrin and vitamin B12 by > 90%, corresponding to a size-cutoff of 1.5 nm and a molecular weight cutoff off (MWCO) of ~1000 g/mol. This size is representative of dyes, peptides, biomacromolecules, and larger pharmaceutical compounds.⁵⁸ By fitting membrane neutral solute rejection data to the DSPM, 40,41 we calculated an effective pore size of 1.95 nm (solid line of Figure 4b, Supporting Information). Given the similar neutral solute rejections observed in Figure 4a, these results are assumed to be representative of the ZAC-0 and CZAC-1 membranes.

3.6. Effect of Acidic Repeat Unit on Charged Solute **Selectivity.** We hypothesized that the hydrophilic nanochannels of the CZAC membranes would be negatively charged due to the deprotonation of MAA in water (Scheme 1b). This was expected to enhance the rejection of charged solutes through Donnan exclusion. 10,47,59,60 According to Donnan theory, a fixed negative charge in the pore simultaneously decreases the partitioning of anionic solutes and increases the partitioning of cationic solutes through electrostatic forces. 40,41 Since electroneutrality requires that the net-charge flux through the membrane is zero, the low concentration of anions ultimately limits salt permeation rate and thus increases rejection. 40,41 Size exclusion is not expected to significantly affect salt rejection for the CZAC membranes, because the effective membrane pore size (~1.95 nm, Figure 4) is much larger than the hydrated diameters of the ions investigated in this work.⁶¹

To determine if Donnan exclusion influences salt rejection, we filtered 5 mM solutions of Na2SO4, CaSO4, and NaCl through the ZAC-0, CZAC-1, and CZAC-2 membranes (Figure 5a). For the CZAC membranes, we observed the trend $R(Na_2SO_4) > R(CaSO_4) \sim R(NaCl)$. This reflects the rejection trend predicted by Donnan theory for a negatively charged membrane.⁵⁹ Interestingly, we observed this same rejection trend for ZAC-0, although to a much lower extent. Many commercial UF membranes, including those we use as supports for ZAC-based TFC membranes here, have negatively charged surfaces to improve their fouling resistance and wettability when used as is. This is supported by reported ζ potential measurements of UE50⁶² and many other PES membranes. 63,64 This is in agreement with our measurements of the rejection of Na₂SO₄ by uncoated UE50 (Figure S3), which can reach to >80% in dilute salt solutions and decreases substantially with increasing feed concentration. These results confirm the presence of a negative membrane charge according to Donnan theory. 40,41,47 While R(Na₂SO₄) was only 15% for the support membrane at 5 mM feed concentration (Figure S3), we speculate that the negative charge of the support led to the slight Donnan exclusion observed for the ZAC-0 TFC membranes.

The CZAC-1 and CZAC-2 membranes demonstrated higher salt rejection than the ZAC-0 membranes, especially for Na_2SO_4 (Figure 5a). Since the three membranes had similar size-based selectivity, this suggests that deprotonated MAA

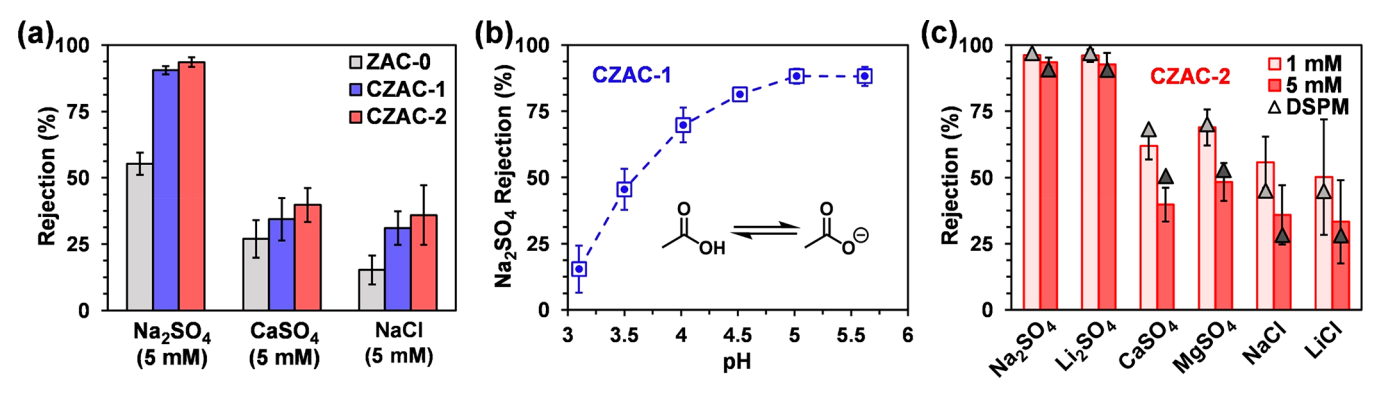


Figure 5. (a) Rejection of 5 mM Na₂SO₄ by ZAC-0, CZAC-1, and CZAC-2 membranes. The greater salt rejection observed for the CZAC TFC membranes is attributed to negative charge conferred by the deprotonated MAA groups. (b) Rejection of 5 mM Na₂SO₄ with varying pH by the CZAC-1 membranes. The fraction of deprotonated MAA groups decreased with decreasing pH, resulting in lower salt retention. The dashed line serves to guide the eye. (c) Rejection of various salts at concentrations of 1 mM and 5 mM by the CZAC-2 membranes. The rejections are fitted to the DSPM using a single anionic charge density for each feed concentration (1 mM: $D_p = 1.95$ nm and $\chi = 21.4$ mM; 5 mM: $D_p = 1.95$ nm and $\chi = 60.4$ mM). The error bars appearing in part a—c are the 95% confidence interval calculated using Student's *t*-distribution.

granted negative charge to CZAC membranes (Scheme 1b).⁵⁹ Interestingly, the CZAC-1 and CZAC-2 membranes demonstrated quite similar rejections of Na₂SO₄, CaSO₄, and NaCl at feed concentrations of 5 mM (Figure 5a) and 1 mM (Figure S4), despite the different compositions of the CZAC selective layers (Figure 1b, Table 1). Since Donnan exclusion is highly dependent on fixed charge density, 40,41,47 this result might suggest that increasing MAA content above 7.0 wt % did not significantly increase the partitioning of MAA into the hydrophilic nanochannels, with additional MAA groups instead partitioning into the hydrophobic nanodomain. However, it is also possible that counterion condensation⁶⁵ resulted in a lower effective charge concentration of the hydrophilic nanochannels for terpolymers with MAA content above 7.0 wt %. If deprotonated MAA enhances salt rejection by conferring negative charge to the hydrophilic nanochannels, then salt rejection should decrease with decreasing pH. Acidbase equilibrium favors protonated MAA under acidic conditions, so the nanochannels would become less anionic at sufficiently low pH.66 To test this, we filtered 5 mM solutions of Na₂SO₄ with varying pH through the CZAC-1 membranes (Figure 5b). As expected, R(Na2SO4) steadily decreased from $\sim 90\%$ at pH 5.0-5.6 to $\sim 15\%$ at pH 3.1, indicating the equilibrium shift from deprotonated to protonated MAA.⁶⁷ The reported pK_a of PMAA is 4.8,⁶⁸ so we expect that most of the MAA groups were protonated at the lowest pH of 3.1. As a result, salt rejection was negligible without the negative charge conferred by the carboxylate groups. Interestingly, CZAC-1 membrane permeance while filtering the pH 3.1 solution was the same as with deionized water (Figure S5). A decrease in permeance would reflect deswelling of the hydrophilic nanochannels through collapse of the protonated PMAA segments; 59,67 however, this was not observed for our system.

Further investigation of the hysteretic behavior of acidic CZACs in respond to pH changes would be quite interesting, as this has been observed for self-assembled triblock copolymer membranes possessing PMAA pore-internal blocks. For the filtration experiments represented in Figure 5b, pH was chronologically adjusted as pH 5.6, pH 4.5, pH 3.5, pH 3.1, pH 4.0, and finally pH 5.0. Given the similar rejections observed for pH 5.6 and pH 5.0, it is unlikely that CZAC-1 membranes demonstrated hysteretic behavior within the pH

window of 3.1–5.6. This does not preclude hysteric behavior at higher pH values, which we did not investigate.

As mentioned previously, the low salt rejection observed at pH 3.1 indicates that salt rejection was negligible without the negative charge conferred by the carboxylate groups. This result also implies that dielectric exclusion, defined as reduced ion partitioning due to a low dielectric constant of the membrane system, 40,66 did not strongly influence salt rejection. PA-TFC membranes, in contrast, rely heavily on dielectric exclusion to achieve high salt retention. We speculate that the absence of dielectric exclusion was due to the larger pore size and the polarity/ hydrophilicity of the zwitterions. 69

To further investigate CZAC membrane selectivity, we systematically tested the effect of z_1/z_2 pairing (e.g. +1/-2 for Na₂SO₄), feed concentration, and cation species on salt rejection for the CZAC-2 membranes (Figure 5c). Salt rejection was most strongly determined by the z_1/z_2 pairing, consistent with the predictions from Donnan theory. We observed lower salt rejections at higher feed concentrations, also consistent with Donnan theory. The cation species did not affect selectivity beyond its determination of z_1/z_2 pairing (e.g., $R(\text{Na}_2\text{SO}_4) = R(\text{Li}_2\text{SO}_4)$). This result is again consistent with Donnan theory. Furthermore, this last result suggests that selective SBMA-cation and MAA-cation interactions did not influence selectivity for the salts that were investigated.

We fit the rejection of the 1 and 5 mM salts by the CZAC-2 membranes using the DSPM (Figure 5c). For each feed concentration, we fit a single anionic charge density (χ) assuming the same effective pore diameter (~1.95 nm) determined by neutral solute rejection⁴⁰ (Figure 4b). We measured consistent membrane permeance during the salt filtration experiments (Figure S6), which supports this assumption. We fit membrane charge densities of $\chi = 21.4$ mM and $\chi = 60.4$ mM for 1 and 5 mM feed solution concentrations, respectively. Salt rejection depends on the ratio of membrane charge density to feed concentration (i.e., χ / C_{Feed}), 40 so the higher salt rejections observed for the 1 mM feed solutions were consistent with our fit to the DSPM. However, it is presently unclear why χ increased with feed concentration. This trend can artificially occur when salt rejection resulting from dielectric exclusion is falsely attributed to Donnan exclusion, 40 but the low Na₂SO₄ rejection at pH 3.1 suggests that dielectric exclusion was unimportant for our

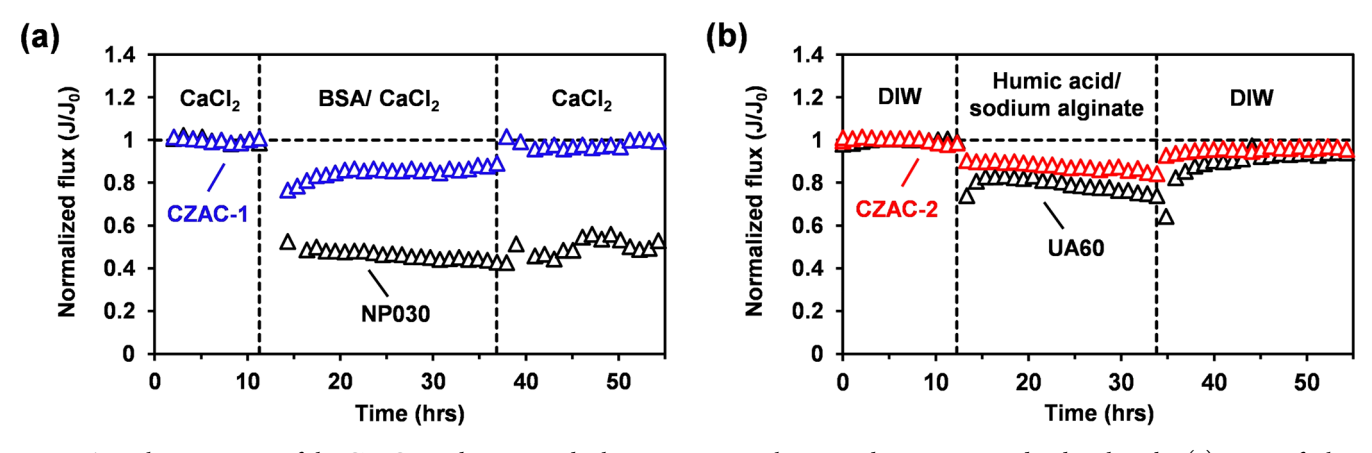


Figure 6. Fouling resistance of the CZAC membranes. For both tests, commercial NF membranes were used as benchmarks. (a) Protein fouling test (1000 ppm BSA, 10 mM CaCl₂, pH 6.3, $J_0 = 5.4$ L m⁻² h⁻¹) performed using the CZAC-1 and NP030 membranes. (b) Organic fouling test (1000 ppm humic acid, 1000 ppm sodium alginate, pH 4.5, $J_0 = 8.1$ L m⁻² h⁻¹) performed using the CZAC-2 and UA60 membranes.

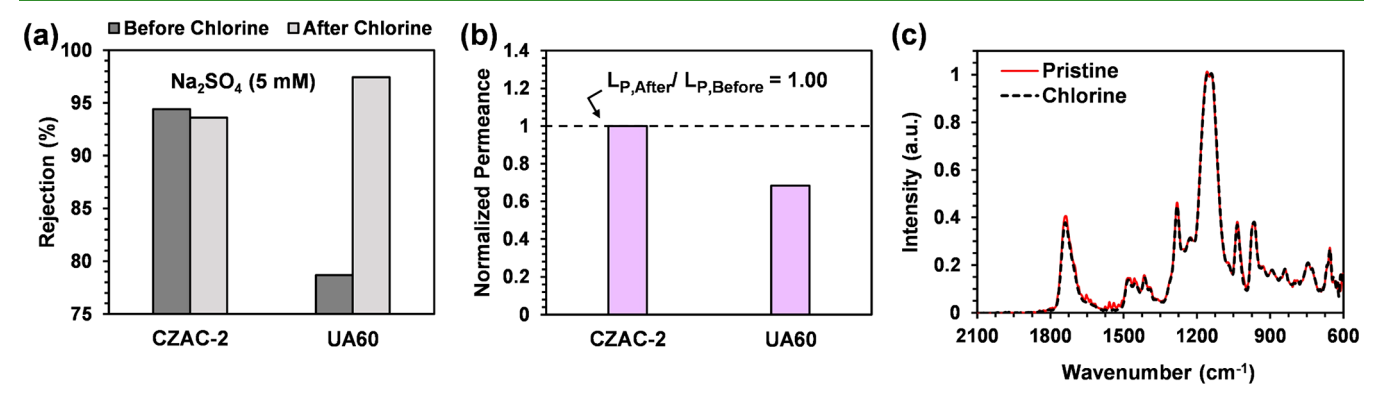


Figure 7. Effect of chlorine exposure on (a, b) CZAC-2 and UA60 membrane performance and (c) CZAC-2 terpolymer bond chemistry. The chlorine dosage was 32 000 ppm·h (2000 ppm sodium hypochlorite, 16 h, pH 4.5). (a) Rejection of 5 mM Na_2SO_4 before and after chlorine exposure. (b) Permeance after chlorine exposure ($L_{P,After}$) normalized by permeance before chlorine exposure ($L_{P,Before}$). (c) ATR-FTIR spectra of CZAC-2 films before (Pristine) and after (Chlorine) chlorine exposure. No discernible change to terpolymer bond chemistry indicates resistance to chlorine attack.

system. We speculate that the effective charge density increased with feed concentration due to the solvated ions breaking SBMA-MAA complexes through competitive binding, reducing interchain charge screening. However, this is difficult to verify experimentally.

3.7. Membrane Fouling Resistance. Management of membrane fouling is a crucial operational task, largely determining membrane lifetime and performance. To determine fouling resistance, we tracked flux at a given pressure while filtering model foulants in dead-end mode. At the end of the fouling period, we gently rinsed the membranes with the background electrolyte solution and measured the final water flux to determine the reversibility of the fouling. We benchmarked CZAC TFC membrane performance with commercial NF membranes, the NP030 (PES, Microdyne) and the UA60 (piperazine-based PA, Trisep). These benchmarks were selected because their salt rejection is similar to that of the CZAC membranes. PA and PES membrane chemistries were selected to access a wider breadth of membrane surface properties.

CZAC-1 membranes demonstrated excellent fouling resistance when challenged with a solution of BSA (1000 ppm) and $CaCl_2$ (10 mM) (Figure 6a), a highly fouling-prone protein system. $CaCl_2$ was included to increase fouling propensity through calcium bridging.⁴⁴ The fouling test was carried out at pH 6.3 to ensure that the MAA groups were deprotonated and

therefore able to participate in calcium bridge formation. CZAC-1 membranes showed minimal flux decline during the 24 h fouling period, likely due to cake deposition, and almost complete flux recovery (98%) after a simple rinse (Figure 6a). These results demonstrate excellent resistance to protein fouling. The NP030, a commercial PES NF membrane used as benchmark, showed significant flux decline during the fouling experiment and only 50% flux recovery.

The CZAC-2 membranes demonstrated excellent fouling resistance when challenged with a solution of humic acid (1000 ppm) and sodium alginate (1000 ppm) (Figure 6b), an organic mixture containing key organic foulants in surface water, wastewater streams, and seawater.^{72–74} The pH was reduced to 4.5 to increase the fouling propensity.⁴⁵ We chose not to include calcium, which increases fouling propensity through bridging similarly to BSA,⁴⁵ because calcium was already used for the BSA fouling experiments. CZAC-2 membranes showed minimal flux decline during the 20-h fouling period and almost completely recovered their initial water flux (96%) after a simple rinse (Figure 6b). The UA60, a commercial piperazine-based PA-TFC used as a benchmark, showed larger flux decline during the fouling period and a lower flux recovery (93%).

3.8. Chlorine Tolerance. Management of biofouling is crucial for maintaining membrane lifetime and performance. 13,22 Chlorine exposure is the preferred method for

disinfection due to its low cost and simplicity, but polyamide TFC membranes are highly sensitive to chlorine degradation. ^{13,22,24} This necessitates alternative methods for biofouling control, substantially adding to cost and system complexity. ¹³ The CZACs used in this work possessed chemical bonds that are resistant to oxidation, suggesting that CZAC TFC membranes would remain stable upon chlorine treatment. To test this, we exposed the CZAC-2 membranes to a concentrated (2000 ppm) solution of sodium hypochlorite for 16 h (32 000 ppm·h). We adjusted the pH to 4.5 using HCl to ensure that hypochlorous acid was the dominant chlorine species. ²² Most NF and RO plants operate under mildly acidic conditions to reduce scaling, so this was a realistic condition for chlorine exposure. ²²

To determine the effect of chlorine treatment on membrane performance, we first examined rejection of 5 mM Na₂SO₄ (Figure 7a) and permeance (Figure 7b) before and after chlorine exposure. Membrane permeance after chlorine treatment $(L_{P,After})$ was normalized by the initial permeance before chlorine treatment $(L_{P,Before})$. For the CZAC-2 membrane, Na₂SO₄ rejection decreased slightly from 94.4% to 93.6% (Figure 7a) with no measurable change in permeance (Figure 7b, $L_{P,After}/L_{P,Before} = 1.00$). These results demonstrate that the CZAC-2 membranes maintained consistent selectivity and permeance upon intense chlorine exposure. To establish a benchmark, we subjected the UA60, a commercial piperazinebased PA-TFC, to identical chlorine treatment. The UA60 demonstrated unacceptable changes to performance, with Na₂SO₄ rejection increasing from 79% to 97.8% (Figure 7a) and permeance decreasing to 68% of its initial value (Figure 7b, $L_{P,After}/L_{P,Before} = 0.68$). These decreases can be at least partially attributed to increased hydrophobicity resulting from chlorination.²² These results illustrate that the CZAC-2 membranes were far more resistant to chlorine treatment than the commercial PA-TFC benchmark.

To determine the effect of chlorine exposure on CZAC-2 bond chemistry, we performed the same chlorine treatment on ${\sim}50~\mu m$ CZAC-2 films and examined the bond chemistry using ATR-FTIR (Figure 7b). We observed no difference between the spectra of the pristine and chlorine-treated films, indicating that new bonds did not form due to chlorine attack. This result further suggests that the CZACs investigated in this work possessed stable chemical bonds that remain stable upon chlorine exposure. ATR-FTIR also confirmed stable CZAC-2 ester bond chemistry after 24 h of exposure to pH 1.0–3.0 solutions (Figure S7), suggesting that the CZAC membranes were also resistant to acid-catalyzed hydrolysis. The catalogue of the confirmed stable catalogue of the catalogue of the catalogue of the catalogue of the catalogue of catalogue of the catalogue of catalogue o

4. CONCLUSIONS

This work introduces CZACs, random terpolymers of hydrophobic, zwitterionic, and acidic/ionizable repeat units to develop self-assembled NF membranes. We show that CZAC TFC membranes and analogous uncharged r-ZAC TFC membranes exhibit identical size-based selectivity, suggesting that the ionizable repeat units dos not affect the self-assembled pore size. In contrast, we demonstrate that the ionized acidic group confers negative charge to the CZAC membranes, thereby enhancing salt rejection through Donnan exclusion. Salt rejection is successfully modeled using the Donnan Steric Pore Model. These CZAC membranes demonstrate excellent resistance to fouling by proteins and organic macromolecules, illustrating their potential for treating challenging fouling-

prone feedstocks. This robust polymer chemistry also enables high chlorine tolerance, with negligible changes in membrane performance upon exposure to chlorine (32 000 ppm·h). Overall, this work offers a promising approach to developing water filtration membranes with NF-type selectivity and excellent fouling and chlorine resistance.

ASSOCIATED CONTENT

Supporting Information

The Supporting Information is available free of charge at https://pubs.acs.org/doi/10.1021/acsapm.1c01940.

Materials, terpolymer ¹H NMR, salt rejection at 1 mM feed concentration, permeance during salt filtration, and DSPM for neutral solutes and salts (PDF)

AUTHOR INFORMATION

Corresponding Author

Ayse Asatekin — Department of Chemical and Biological Engineering, Tufts University, Medford, Massachusetts 02155, United States; orcid.org/0000-0002-4704-1542; Email: ayse.asatekin@tufts.edu

Author

Samuel J. Lounder — Department of Chemical and Biological Engineering, Tufts University, Medford, Massachusetts 02155, United States

Complete contact information is available at: https://pubs.acs.org/10.1021/acsapm.1c01940

Notes

The authors declare the following competing financial interest(s): Ayse Asatekin owns a minor equity in and serves as the Senior Scientific Advisor of ZwitterCo. Inc., which was the lead institution in NSF Grant IIP-1843847 that partially funded this work. ZwitterCo. also holds a license from Tufts University to commercialize the technology described in this manuscript. Samuel J. Lounder declares no conflict of interest.

ACKNOWLEDGMENTS

We gratefully acknowledge financial support from the National Science Foundation (NSF) under Grant Number CBET-1553661 and under Grant Number IIP-1843847 led by ZwitterCo, Inc. A.A. thanks Chris Drover for helpful conversations regarding the potential commercial applications and scale-up processes for this technology.

■ REFERENCES

ı

- (1) Werber, J. R.; Osuji, C. O.; Elimelech, M. Materials for next-generation desalination and water purification membranes. *Nature Reviews Materials* **2016**, *1* (5), 1–15.
- (2) Mauter, M. S.; Zucker, I.; Perreault, F. O.; Werber, J. R.; Kim, J.-H.; Elimelech, M. The role of nanotechnology in tackling global water challenges. *Nature Sustainability* **2018**, *1*, 166–175.
- (3) Van der Bruggen, B. Sustainable implementation of innovative technologies for water purification. *Nature Reviews Chemistry* **2021**, *5*, 217–218.
- (4) Greenlee, L. F.; Lawler, D. F.; Freeman, B. D.; Marrot, B.; Moulin, P. Reverse osmosis desalination: water sources, technology, and today's challenges. *Water Res.* **2009**, *43* (9), 2317–2348.
- (5) Moon, J. D.; Freeman, B. D.; Hawker, C. J.; Segalman, R. A. Can Self-Assembly Address the Permeability/Selectivity Trade-Offs in Polymer Membranes? *Macromolecules* **2020**, *53* (14), 5649–5654.

- (6) Shannon, M. A.; Bohn, P. W.; Elimelech, M.; Georgiadis, J. G.; Marinas, B. J.; Mayes, A. M. Science and technology for water purification in the coming decades. *Nature* **2008**, *452*, 301–310.
- (7) Lewis, S. R.; Datta, S.; Gui, M.; Coker, E. L.; Huggins, F. E.; Daunert, S.; Bachas, L.; Bhattacharyya, D. Reactive nanostructured membranes for water purification. *Proceedings of the National Academy of Sciences of the United States of America* **2011**, 108 (21), 8577–8582.
- (8) Lee, K. P.; Arnot, T. C.; Mattia, D. A review of reverse osmosis membrane materials for desalination Development to date and future potential. *J. Membr. Sci.* **2011**, 370 (1–2), 1–22.
- (9) Van der Bruggen, B.; Vandecasteele, C. Removal of pollutants from surface water and groundwater by nanofiltration: overview of possible applications in the drinking water industry. *Environ. Pollut.* **2003**, *122*, 435–445.
- (10) Hoffman, J. R.; Phillip, W. A. Dual-Functional Nanofiltration Membranes Exhibit Multifaceted Ion Rejection and Antifouling Performance. ACS Applied Materials & Interfaces 2020, 12 (17), 19944–19954.
- (11) Bader, M. S. H. Sulfate removal technologies for oil fields seawater injection operations. *Journal of Petroleum Science and Engineering* **2007**, 55 (1–2), 93–110.
- (12) Petersen, R. J. Composite Reverse Osmosis and Nanofiltration Membranes. J. Membr. Sci. 1993, 83 (1), 81–150.
- (13) Yao, Y.; Zhang, P.; Jiang, C.; DuChanois, R. M.; Zhang, X.; Elimelech, M. High performance polyester reverse osmosis desalination membrane with chlorine resistance. *Nature Sustainability* **2021**, *4*, 138–146.
- (14) Zhang, R.; Liu, Y.; He, M.; Su, Y.; Zhao, X.; Elimelech, M.; Jiang, Z. Antifouling membranes for sustainable water purification: strategies and mechanisms. *Chemical Society Reviews* **2016**, *45* (21), 5888–5924.
- (15) Bengani-Lutz, P.; Zaf, R. D.; Culfaz-Emecen, P. Z.; Asatekin, A. Extremely fouling resistant zwitterionic copolymer membranes with \sim 1 nm pore size for treating municipal, oily and textile wastewater streams. *J. Membr. Sci.* **2017**, *543*, 184–194.
- (16) Arumugham, T.; Kaleekkal, N. J.; Gopal, S.; Nambikkattu, J.; K, R.; Aboulella, A. M.; Ranil Wickramasinghe, S.; Banat, F. Recent developments in porous ceramic membranes for wastewater treatment and desalination: A review. *Journal of Environmental Management* **2021**, 293, 112925.
- (17) Chiao, Y. H.; Chen, S. T.; Yap Ang, M. B. M.; Patra, T.; Castilla-Casadiego, D. A.; Fan, R.; Almodovar, J.; Hung, W. S.; Wickramasinghe, S. R. High-Performance Polyacrylic Acid-Grafted PVDF Nanofiltration Membrane with Good Antifouling Property for the Textile Industry. *Polymers* **2020**, *12* (11), 2443.
- (18) Chiao, Y. H.; Yap Ang, M. B. M.; Huang, Y. X.; DePaz, S. S.; Chang, Y.; Almodovar, J.; Wickramasinghe, S. R. A "Graft to" Electrospun Zwitterionic Bilayer Membrane for the Separation of Hydraulic Fracturing-Produced Water via Membrane Distillation. *Membranes* 2020, 10 (12), 402.
- (19) Kharraz, J. A.; Farid, M. U.; Jassby, D.; An, A. K. A systematic study on the impact of feed composition and substrate wettability on wetting and fouling of omniphobic and janus membranes in membrane distillation. *J. Membr. Sci.* **2022**, *641*, 119873.
- (20) Zeng, Z.; Yu, D.; He, Z.; Liu, J.; Xiao, F.-X.; Zhang, Y.; Wang, R.; Bhattacharyya, D.; Tan, T. T. Y. Graphene Oxide Quantum Dots Covalently Functionalized PVDF Membrane with Significantly-Enhanced Bactericidal and Antibiofouling Performances. *Scientific Reports* 2016, 6, 20142.
- (21) Keller, A. A.; Su, Y.; Jassby, D. Direct Potable Reuse: Are We Ready? A Review of Technological, Economic, and Environmental Considerations. *ACS ES&T Engineering* **2021**, DOI: 10.1021/acsestengg.1c00258.
- (22) Do, V. T.; Tang, C. Y.; Reinhard, M.; Leckie, J. O. Degradation of Polyamide Nanofiltration and Reverse Osmosis Membranes by Hypochlorite. *Environ. Sci. Technol.* **2012**, *46* (2), 852–859.
- (23) Zhu, X.; Jassby, D. Electroactive Membranes for Water Treatment: Enhanced Treatment Functionalities, Energy Consid-

- erations, and Future Challenges. Acc. Chem. Res. **2019**, 52 (5), 1177–1186.
- (24) Dugas, M. P.; Van Every, G.; Park, B.; Hoffman, J. R.; LaRue, R. J.; Bush, A. M.; Zhang, Y.; Schaefer, J. L.; Latulippe, D. R.; Phillip, W. A. Resilient hollow fiber nanofiltration membranes fabricated from crosslinkable phase-separated copolymers. *Molecular Systems Design & Engineering* 2020, 5 (5), 943–953.
- (25) Barbey, R.; Lavanant, L.; Paripovic, D.; Schuwer, N.; Sugnaux, C.; Tugulu, S.; Klok, H.-A. Polymer Brushes via Surface-Initiated Controlled Radical Polymerization: Synthesis, Characterization, Properties, and Applications. *Chemical Reviews* **2009**, *109*, 5437–5527.
- (26) Van Wagner, E. M.; Sagle, A. C.; Sharma, M. M.; La, Y.-H.; Freeman, B. D. Surface modification of commercial polyamide desalination membranes using poly(ethylene glycol) diglycidyl ether to enhance membrane fouling resistance. *J. Membr. Sci.* **2011**, 367 (1–2), 273–287.
- (27) Verbeke, R.; Gómez, V.; Vankelecom, I. F. J. Chlorine-resistance of reverse osmosis (RO) polyamide membranes. *Prog. Polym. Sci.* **2017**, 72, 1–15.
- (28) Sewerin, T.; Elshof, M. G.; Matencio, S.; Boerrigter, M.; Yu, J.; de Grooth, J. Advances and Applications of Hollow Fiber Nanofiltration Membranes: A Review. *Membranes* **2021**, *11* (11), 890.
- (29) Ilyas, S.; English, R.; Aimar, P.; Lahitte, J.-F.; de Vos, W. M. Preparation of multifunctional hollow fiber nanofiltration membranes by dynamic assembly of weak polyelectrolyte multilayers. *Colloids and Surfaces A: Physicochemical and Engineering Aspects* **2017**, 533, 286–205
- (30) Joseph, N.; Ahmadiannamini, P.; Hoogenboom, R.; Vankelecom, I. F. J. Layer-by-layer preparation of polyelectrolyte multilayer membranes for separation. *Polymer Chemistry* **2014**, *5* (6), 1817–1831.
- (31) Petrila, L. M.; Bucatariu, F.; Mihai, M.; Teodosiu, C. Polyelectrolyte Multilayers: An Overview on Fabrication, Properties, and Biomedical and Environmental Applications. *Materials* **2021**, *14* (15), 4152.
- (32) Brown, R. H.; Duncan, A. J.; Choi, J. H.; Park, J. K.; Wu, T.; Leo, D. J.; Winey, K. I.; Moore, R. B.; Long, T. E. Effect of ionic liquid on mechanical properties and morphology of zwitterionic copolymer membranes. *Macromolecules* **2010**, *43* (2), 790–796.
- (33) Ehrmann, M.; Galin, J. C.; Meurer, B. Statistical n-Butyl Acrylate—Sulfopropyl Betaine Copolymers. 3. Domain Size Determination by Solid-State NMR Spectroscopy. *Macromolecules* **1993**, 26 (5), 988–993.
- (34) Ehrmann, M.; Mathis, A.; Meurer, B.; Scheer, M.; Galin, J. C. Statistical n-Butyl Acrylate-(Sulfopropyl) ammonium Betaine Copolymers. 2. Structural Studies. *Macromolecules* **1992**, 25 (8), 2253–2261.
- (35) Ehrmann, M.; Muller, R.; Galin, J. C.; Bazuin, C. G. Statistical n-Butyl Acrylate-(Sulfopropyl)ammonium Betaine Copolymers. 4. Dynamic Mechanical Properties. *Macromolecules* **1993**, 26 (18), 4910–4918.
- (36) Bengani, P.; Kou, Y.; Asatekin, A. Zwitterionic copolymer self-assembly for fouling resistant, high flux membranes with size-based small molecule selectivity. *J. Membr. Sci.* **2015**, *493*, 755–765.
- (37) Bengani-Lutz, P.; Converse, E.; Cebe, P.; Asatekin, A. Self-Assembling Zwitterionic Copolymers as Membrane Selective Layers with Excellent Fouling Resistance: Effect of Zwitterion Chemistry. ACS Applied Materials and Interfaces 2017, 9 (24), 20859–20872.
- (38) Lounder, S. J.; Asatekin, A. Interaction-based ion selectivity exhibited by self-assembled, cross-linked zwitterionic copolymer membranes. *Proceedings of the National Academy of Sciences of the United States of America* **2021**, 118 (37), No. e2022198118.
- (39) Lounder, S. J.; Asatekin, A. Zwitterionic Ion-Selective Membranes with Tunable Subnanometer Pores and Excellent Fouling Resistance. *Chem. Mater.* **2021**, 33 (12), 4408–4416.
- (40) Bowen, R.; Welfoot, J. S. Modelling the performance of membrane nanofiltration—critical assessment and model development. *Chem. Eng. Sci.* **2002**, *57* (7), 1121–1137.

- (41) Bowen, W. R.; Mohammad, A. W. Diafiltration by nanofiltration: Prediction and optimization. *AIChE J.* **1998**, *44* (8), 1799–1812
- (42) Kolarik, J.; Stol, M. Relaxation Behaviour of Poly(methacrylic acid) and Its Copolymers with 2-Hydroxyethyl Methacrylate. *Polymer Journal* **1973**, *5* (2), 158–163.
- (43) Dechadilok, P.; Deen, W. M. Hindrance Factors for Diffusion and Convection in Pores. *Ind. Eng. Chem. Res.* **2006**, 45 (21), 6953–6959.
- (44) Mo, H.; Tay, K. G.; Ng, H. Y. Fouling of reverse osmosis membrane by protein (BSA): Effects of pH, calcium, magnesium, ionic strength and temperature. *J. Membr. Sci.* **2008**, 315 (1–2), 28–35
- (45) Tang, C. Y.; Kwon, Y.-N.; Leckie, J. O. Fouling of reverse osmosis and nanofiltration membranes by humic acid—Effects of solution composition and hydrodynamic conditions. *J. Membr. Sci.* **2007**, 290 (1–2), 86–94.
- (46) Sadeghi, I.; Asatekin, A. Membranes with Functionalized Nanopores for Aromaticity-Based Separation of Small Molecules. ACS Applied Materials & Interfaces 2019, 11 (13), 12854–12862.
- (47) Sadeghi, I.; Kronenberg, J.; Asatekin, A. Selective Transport through Membranes with Charged Nanochannels Formed by Scalable Self-Assembly of Random Copolymer Micelles. *ACS Nano* **2018**, *12* (1), 95–108.
- (48) Pujari, N. S.; Wang, M.; Gonsalves, K. E. Co and terpolymer reactivity ratios of chemically amplified resists. *Polymer* **2017**, *118* (2), 201–214.
- (49) Ji, Y.; Geise, G. M. The Role of Experimental Factors in Membrane Permselectivity Measurements. *Ind. Eng. Chem. Res.* **2017**, 56 (26), 7559–7566.
- (50) Guillen, G. R.; Pan, Y.; Li, M.; Hoek, E. M. V. Preparation and Characterization of Membranes Formed by Nonsolvent Induced Phase Separation: A Review. *Ind. Eng. Chem. Res.* **2011**, *50* (7), 3798–3817
- (51) Hilal, N.; Al-Zoubi, H.; Darwish, N. A.; Mohammad, A. W. Nanofiltration of magnesium chloride, sodium carbonate, and calcium sulphate in salt solutions. *Sep. Sci. Technol.* **2005**, 40 (16), 3299–3321
- (52) Stevens, D. M.; Shu, J. Y.; Reichert, M.; Roy, A. Next-Generation Nanoporous Materials: Progress and Prospects for Reverse Osmosis and Nanofiltration. *Ind. Eng. Chem. Res.* **2017**, *56* (38), 10526–10551.
- (53) Carter, B. M.; Wiesenauer, B. R.; Hatakeyama, E. S.; Barton, J. L.; Noble, R. D.; Gin, D. L. Glycerol-based bicontinuous cubic lyotropic liquid crystal monomer system for the fabrication of thin-film membranes with uniform nanopores. *Chem. Mater.* **2012**, 24 (21), 4005–4007.
- (54) Dischinger, S. M.; Rosenblum, J.; Noble, R. D.; Gin, D. L.; Linden, K. G. Application of a lyotropic liquid crystal nanofiltration membrane for hydraulic fracturing flowback water: Selectivity and implications for treatment. *J. Membr. Sci.* **2017**, *543*, 319–327.
- (55) Bengani-Lutz, P.; Sadeghi, I.; Lounder, S. J.; Panzer, M. J.; Asatekin, A. High Flux Membranes with Ultrathin Zwitterionic Copolymer Selective Layers with ~1 nm Pores Using an Ionic Liquid Cosolvent. ACS Applied Polymer Materials 2019, 1 (8), 1954–1959.
- (56) Qian, X.; Ravindran, T.; Lounder, S. J.; Asatekin, A.; McCutcheon, J. R. Printing zwitterionic self-assembled thin film composite membranes: Tuning thickness leads to remarkable permeability for nanofiltration. *J. Membr. Sci.* **2021**, 635, 119428.
- (57) Liang, Y.; Zhu, Y.; Liu, C.; Lee, K.-R.; Hung, W.-S.; Wang, Z.; Li, Y.; Elimelech, M.; Jin, J.; Lin, S. Polyamide nanofiltration membrane with highly uniform sub-nanometre pores for sub-1 A precision separation. *Nature Communications* **2020**, *11*, 2015.
- (58) Marchetti, P.; Jimenez Solomon, M. F.; Szekely, G.; Livingston, A. G. Molecular separation with organic solvent nanofiltration: A critical review. *Chemical Reviews* **2014**, *114* (21), 10735–10806.
- (59) Qu, S.; Dilenschneider, T.; Phillip, W. A. Preparation of Chemically-Tailored Copolymer Membranes with Tunable Ion

- Transport Properties. ACS Applied Materials and Interfaces 2015, 7 (35), 19746-19754.
- (60) Léniz-Pizarro, F.; Liu, C.; Colburn, A.; Escobar, I. C.; Bhattacharyya, D. Positively charged nanofiltration membrane synthesis, transport models, and lanthanides separation. *J. Membr. Sci.* **2021**, *620*, 118973.
- (61) Nightingale, E. R. Phenomenological theory of ion solvation. Effective radii of hydrated ions. *J. Phys. Chem.* **1959**, *63* (9), 1381–1387.
- (62) Zhu, J.; Zheng, J.; Zhang, Q.; Zhang, S. Antifouling ultrafiltration membrane fabricated from poly (arylene ether ketone) bearing hydrophilic hydroxyl groups. *J. Appl. Polym. Sci.* **2016**, *133* (1), 42809–42820.
- (63) Burns, D. B.; Zydney, A. L. Buffer effects on the zeta potential of ultrafiltration membrane. *J. Membr. Sci.* **2000**, *172* (1–2), 39–48.
- (64) Najjar, A.; Sabri, S.; Al-Gaashani, R.; Atieh, M. A.; Kochkodan, V. Antibiofouling Performance by Polyethersulfone Membranes Cast with Oxidized Multiwalled Carbon Nanotubes and Arabic Gum. *Membranes* **2019**, 9 (2), 32.
- (65) Kamcev, J.; Paul, D. R.; Manning, G. S.; Freeman, B. D. Ion Diffusion Coefficients in Ion Exchange Membranes: Significance of Counterion Condensation. *Macromolecules* **2018**, *51* (15), 5519–5529.
- (66) Epsztein, R.; Shaulsky, E.; Dizge, N.; Warsinger, D. M.; Elimelech, M. Role of Ionic Charge Density in Donnan Exclusion of Monovalent Anions by Nanofiltration. *Environ. Sci. Technol.* **2018**, 52 (7), 4108–4116.
- (67) Weidman, J. L.; Mulvenna, R. A.; Boudouris, B. W.; Phillip, W. A. Unusually Stable Hysteresis in the pH-Response of Poly(Acrylic Acid) Brushes Confined within Nanoporous Block Polymer Thin Films. J. Am. Chem. Soc. 2016, 138 (22), 7030–9.
- (68) Bukenya, M.; Lee, J. H.; Kalidindi, S.; DeCortin, M.; Tice, L.; Yoo, P. J.; Yi, H. A Robust Fabrication Technique for Hydrogel Films Containing Micropatterned Opal Structures via Micromolding and an Integrated Evaporative Deposition-Photopolymerization Approach. *Langmuir* **2021**, *37* (4), 1456–1464.
- (69) Beckstein, O.; Tai, K.; Sansom, M. S. P. Not Ions Alone: Barriers to Ion Permeation in Nanopores and Channels. *J. Am. Chem. Soc.* **2004**, *126*, 14694–14695.
- (70) Trisep DS Food and Dairy NP030 Series. https://www.microdyn-nadir.com/wp-content/uploads/DS-NP030.pdf (accessed February 2, 2022).
- (71) Trisep UA60 NF Membrane for Separation and Purification. https://www.microdyn-nadir.com/wp-content/uploads/UA60-Flat-Sheet-Membrane.pdf (accessed February 2, 2022).
- (72) Jarusutthirak, C.; Amy, G.; Croue, J. P. Fouling characteristics of wastewater effluent organic matter (EfOM) isolates on NF and UF membranes. *Desalination* **2002**, *145* (1–3), 247–255.
- (73) Manttari, M.; Puro, L.; Nuortila-Jokinen, J.; Nystrom, M. Fouling effects of polysaccharides and humic acid in nanofiltration. *J. Membr. Sci.* **2000**, *165* (1), 1–17.
- (74) Li, Q. L.; Elimelech, M. Organic fouling and chemical cleaning of nanofiltration membranes: Measurements and mechanisms. *Environmental Science & Technology* **2004**, 38 (17), 4683–4693.
- (75) Schonemann, E.; Laschewsky, A.; Rosenhahn, A. Exploring the Long-Term Hydrolytic Behavior of Zwitterionic Polymethacrylates and Polymethacrylamides. *Polymers* **2018**, *10* (6), 639.